Available online at www.sciencedirect.com
SCIENCE DIRECT
Polymer 47 (2006) 4649–4658
polymer
www.elsevier.com/locate/polymer

High-pressure CO_2-enhanced polymer interdiffusion and dissolution studied with in situ ATR-FTIR spectroscopic imaging

Oliver S. Fleming, K.L. Andrew Chan, Sergei G. Kazarian *

Department of Chemical Engineering, Imperial College London, South Kensington Campus, London SW7 2AZ, United Kingdom

Received 15 March 2006; accepted 26 April 2006

Abstract

A novel application of attenuated total reflection Fourier transform infrared (ATR-FTIR) spectroscopic imaging to study polymer interdiffusion and dissolution under high-pressure or supercritical carbon dioxide environments has been demonstrated. Miscible systems of polyvinylpyrrolidone (PVP) and poly(ethylene glycol) (PEG) of different molecular weights have been chosen for this investigation. These systems were subjected to a controlled pressure of CO_2 and the interfacial area of contact between the two polymers was studied by ATR-FTIR imaging in situ. Using this spectroscopic imaging approach, the phenomenon of polymer interdiffusion enhanced by CO_2 dissolved in both polymers was investigated as a function of time. The evolution of spatially resolved images as a function of time was studied with FTIR imaging and the corresponding concentration profiles for both polymers were obtained. The chemical specificity of FTIR imaging also allowed us to measure the amount of CO_2 dissolved in each domain of the polymer system. Effects of PEG molecular weight and pressure of CO_2 on the mechanism and the rate of polymer interdiffusion was investigated. This approach has not only shown the ability to visualise the process of interdiffusion but also demonstrated the ability of high-pressure CO_2 to 'tune' the rate of interdiffusion, this information is important for a better understanding of CO_2-induced mixing of polymeric materials.

Keywords: FT-IR imaging; Diffusion; Supercritical fluids

1. Introduction

High-pressure and supercritical CO_2 is a useful processing aid in polymer technology. The relatively high-solubility of CO_2 in glassy polymers and in the amorphous domains of some semi-crystalline polymers is partly the result of CO_2 molecules weakly interacting with the basic sites on the macromolecular chains. The directly related facet of CO_2 solubility is its ability to plasticise the amorphous domains of the polymer matrix. The action of CO_2 molecules to plasticise the matrix to enhance the diffusion of organic dyes into polymer matrix was described as 'molecular lubrication'. The presence of dissolved CO_2 molecules in the polymer matrix is accompanied by an increase in segmental and chain mobility of the polymer, thus effectively mimicking the effect of heat. Important distinctions between CO_2 and conventional plasticisers are the transient nature of the effect and the ease of its removal from polymer at the end of the process. Additionally, control of the polymer free-volume may be achieved by pressure manipulation. The suitability of high-pressure CO_2 processing technology in the pharmaceutical industry is pronounced in the ability to impregnate active pharmaceutical ingredients into the polymer matrix to achieve molecular dispersion in a 'solvent-free' manner [1].

Implications to this favourable interaction of high-pressure CO_2 with glassy and semi-crystalline polymers include viscosity reduction of the bulk polymer phase [2,3], extrusion [4,5], polymer foaming [6,7], and polymer blend formation [8,9]. The benefits that CO_2 provides in these examples may be anticipated to extend to enhancing/accelerating the interdiffusion in miscible polymer systems as a direct consequence of plasticisation and viscosity reduction of the polymer components. Because of the experimental challenges, studies of polymer interdiffusion facilitated by high-pressure CO_2 are limited. Recent examples include the study of self-diffusion of polystyrene [10], low-temperature reactive coupling at polymer–polymer interfaces [11], and studies of density fluctuations in thin polymer films [12] subjected to supercritical CO_2. It should be noted that relevant studies of organic solvent enhanced diffusion of polymers have also been

* Corresponding author. Tel.: +44 207 594 5574; fax: +44 207 594 1989.
E-mail address: s.kazarian@imperial.ac.uk (S.G. Kazarian).

0032-3861/$ - see front matter © 2006 Elsevier Ltd. All rights reserved.
doi:10.1016/j.polymer.2006.04.059

reported recently [13]. Knowledge of CO_2-enhanced interdiffusion in a polymer blend aids the full understanding of this novel processing route and therefore, provides the required knowledge to optimise the technology. Previous attempts to study polymer interdiffusion under high-pressure CO_2 involved rheology, light scattering and neutron reflectivity. To study polymer interdiffusion one would ideally need a chemically specific method combined with the capacity to record spatially resolve information.

FTIR spectroscopic imaging has recently been developed into a powerful experimental tool to study dynamic polymer systems [14–19]. The recent development of ATR imaging using a diamond ATR accessory [20,21] permits the study of various polymer processes under high-pressure CO_2 in situ [22]. This approach was extended to enable a qualitative chemical imaging analysis of polymer systems exposed to high-pressure and supercritical environments [21]. This technique offers a quantitative visualisation tool to study the effect of CO_2 in a dynamic polymer system. Processes may be followed as a function of time and importantly, the molecular interactions driving the observed behaviour may also be detected and interpreted. To evaluate the effect of high-pressure CO_2 on the interdiffusion of a polymer system and the validity of our in situ imaging approach to study the phenomena, a model system was selected where polymer interdiffusion induced by heat has been reported in the literature. The interdiffusion of PEG and PVP has received much attention due to its importance in pharmaceutical formulations [23–26]. Blends of PVP–PEG are used for the preparation of skin patches due to their good adhesive properties to the surface of the skin and the ability to control the diffusion of released drug molecules. Information and conditions regarding the interdiffusion of these polymers, formation of a homogeneous blend and possible phase separation are important phenomenon for optimal design of materials based on these polymers. The effect of molecular weight on the diffusion characteristics of both polymers have been highlighted in studies where interdiffusion was induced by heat and studied via optical wedge microinterferometry [24]. Our in situ study of the PEG–PVP system via ATR-FTIR spectroscopic imaging is the first example of the application of this powerful imaging approach to polymer interdiffusion facilitated by high-pressure or supercritical CO_2.

2. Experimental section

2.1. Polymer interface preparation

PVP (K15, 10,000 M_w), PEG 1500 and PEG 600 were purchased from Sigma, and used as received without further treatment. A film of PVP with 20 wt% of PEG 1500 was created by co-dissolving in ethanol followed by casting directly onto the diamond ATR crystal, which was heated to 90 °C. The necessity for the inclusion of PEG is to ensure good contact between the PVP and the diamond ATR crystal following the evaporation of ethanol. A similar film preparation method was utilised in the related study [23]. After ca. 25 min following polymer solution deposition, a scalpel was used to remove half of the polymer film along the central line across the diamond. The sample was held at 90 °C until all of the ethanol had evaporated, the level of which was monitored via FTIR spectroscopy. Once all of the ethanol was removed, which typically took ca. 45 min, PEG was placed onto the remaining half of the diamond. An intimate and uniform contact between PVP and PEG at the interface has been easily achieved for PEG 600 since it is a liquid at room temperature. For PEG 1500, which is a solid in ambient condition, heat was applied to melt the PEG at ca. 70 °C resulting in good contact between solid PVP and liquid PEG phases. All experiments were prepared using approximately the same quantity of each polymer, thus enabling a fair comparison to be made between experiments. At the point of contact between the polymers, the film thickness was approximately identical, which enables one to study uniaxial diffusion by eliminating potential diffusion from the top of one of the polymer phases.

2.2. High-pressure apparatus

The miniature cell used in this study is the same as that used in our previous investigation [21]; the principle of using this cell for polymer interdiffusion is shown schematically in Fig. 1. The absence of fragile windows and the small volume of the cell result in an inherently safe design. The cell is sealed with a polytetrafluoroethylene (PTFE) spacer against the diamond support plate and is held in position using the gate of the accessory. The temperature in the high-pressure cell can be adjusted using the temperature control unit and was maintained at 35 °C for all experiments so that it was above the critical temperature of CO_2. Once thermal equilibrium was reached, the cell was slowly loaded with CO_2 (99% purity provided by BOC) using an ISCO model 500D syringe pump. Cell pressurisation was typically completed within 1 min and the system pressure was monitored during the pressurisation stage and throughout the course of the experiment using a digital pressure transducer. Once the required pressure was reached,

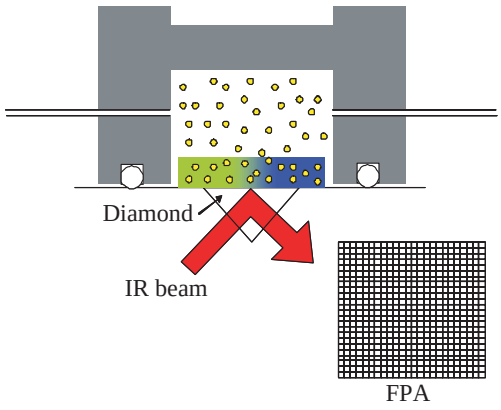

Fig. 1. Schematic diagram of high-pressure cell showing the interface of PVP (green) and PEG (blue) in the presence CO_2 molecules (yellow). The interfacial region of the polymer system covers the diamond ATR crystal.

the image acquisition procedure was initiated, which served as time zero for the interdiffusion experiments.

2.3. FTIR imaging

Fourier transform infrared images were collected using a 64×64 focal plane array (FPA) detector through the diamond ATR accessory in a macro chamber with a step scan spectrometer as described in a previous publication [21]. The ATR imaging approach is patented by Varian [27]. Spectra were recorded using five co-additions with a spectral resolution of 8 cm^{-1}, which took ca. 3 min to acquire an image.

3. Results

3.1. In situ ATR-FTIR imaging approach

The experimental system has been designed to enable interdiffusion to be studied in a uniaxial manner. A straight interface between the two polymers was prepared approximately at the central location of the diamond, which, when imaged, extends vertically from the bottom of the image. The interdiffusion occurring in the polymer system is therefore, observed along the horizontal plane of the image. The studied length scales are dictated by the spatial resolution of ca. 15 μm available with ATR-FTIR imaging using this particular set-up [20]. This is significantly greater than the scales studied by neutron reflectivity and thus, later stages of interdiffusion are studied with ATR-FTIR imaging. The intrinsic vibrational modes associated with the functional groups present on the polymer backbone provide the basis for FTIR spectroscopy to differentiate and characterise polymers. To study the spatial distribution of the components in this ternary system, FTIR spectra of the individual components have to be compared to select suitable spectral bands corresponding to a particular component. The FPA detector provides spatial discrimination and hence images are generated based on the distribution of the integrated absorbance of a specific spectral band, corresponding to either of the components in this ternary PVP/PEG/CO_2 system.

ATR-FTIR spectra of PVP and PEG 600 are presented in Fig. 2, which reveal several regions that are absent from mutual spectral overlap. As mentioned in Section 2, PEG 1500 is added to mildly plasticise PVP. The small quantity of PEG 1500 (20 wt%) in the bulk PVP is detected and characterised by the absorbance in the 1020–1170 cm^{-1} region. Pure PEG 1500 is a semi-crystalline polymer at 35 °C, but a specific interaction occurring between the chains of dispersed PEG and chains of PVP inhibits the formation of PEG crystallites, which is signified by the lack of crystalline PEG absorption at 1060 cm^{-1} [28]. The presence of PVP was identified by the absorbance of the ν (C=O) mode between 1600 and 1720 cm^{-1} and PEG between 1000 and 1175 cm^{-1}. The spectrum of dissolved CO_2 in polymeric material is well characterised [29] and can be identified by the ν_3 band of CO_2 between 2300 and 2350 cm^{-1}.

ATR-FTIR images corresponding to PVP in contact with PEG 600 in the absence of CO_2, at 40 and 80 bar are presented in Fig. 3. The images correspond to an area of ca. 820×1140 μm^2, as determined in a previous study [20], and are accompanied with a scale bar, which associates the colour used in the images with the integrated absorbance. The initial distribution (0 min) is seen to consist of the two polymers in contact with a sharp, straight interface, which typifies all experiments that have been performed. PVP is seen to occupy the left side of the image, interpreted by the high-intensity of the red/pink colour in this region. The right side of the image is initially absent from PVP and is composed entirely of PEG 600. Inspection of the images reveals a cluster of low intensity pixels in the top left hand corner, which appear out of place when one considers the intensity of the surrounding pixels. These correspond to bad pixels that are no longer active due to delamination of the detector elements and were consequently not included in the analysis. In the series of images conducted in the absence of CO_2, PVP is in the solid state in contact with liquid PEG 600 and hence the diffusion process occurs at a glassy/liquid interface and can be viewed as the dissolution of PVP in PEG. Once this interface was formed, the image acquisition procedure was initiated with measurements taken at various times to enable the diffusion (dissolution) of PVP to be visualised. As time progresses, the advance of PVP into the PEG phase (initially absent from PVP) is observed for all series of images. However, the timescale in which the diffusion process takes place depends on the experimental conditions and it is enhanced with the increase of CO_2 pressure.

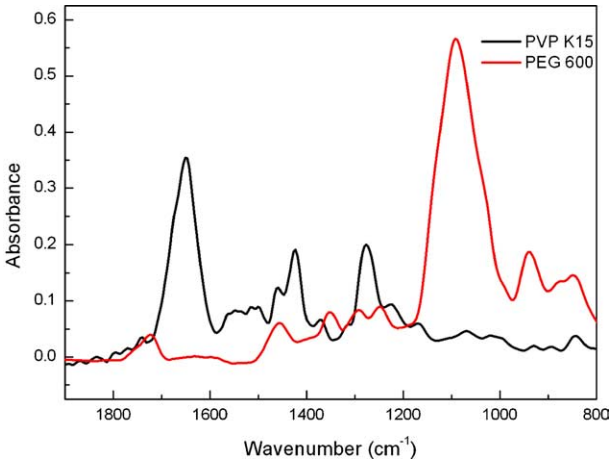

Fig. 2. ATR-FTIR spectra of PVP K15 (black) and PEG 600 (red) measured with 8 cm^{-1} spectral resolution.

3.2. Data analysis

An analysis has been performed to quantify the effect of CO_2 pressure at accelerating the polymer interdiffusion. The diffusion analysis implemented in this study requires the evolution of the spatial concentration profile of one of the polymers as a function of time to be studied. The measured images provide component concentrations in the time and spatial dimension, which is required to assess the diffusion behaviour. The arrangement of the polymer interface on the diamond ATR crystal facilitated the study of the specific

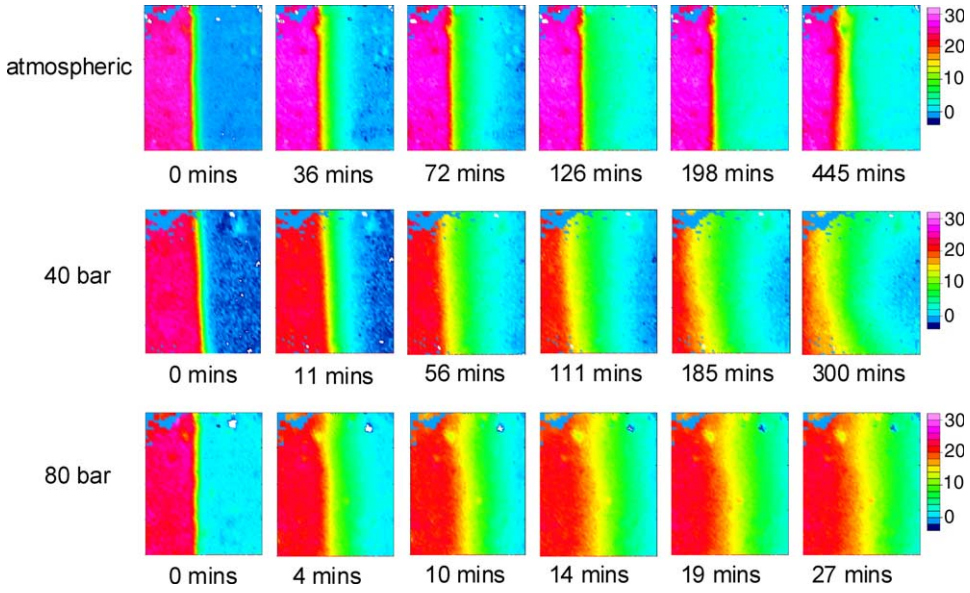

Fig. 3. FTIR-ATR images corresponding to PVP in contact with PEG 600 as a function of pressure. The images are based on the distribution of the integrated absorbance of the carbonyl band of PVP.

component concentration profile of the system along the axis perpendicular to the interface. The evolution of the concentration distribution of a specific component is achieved by extracting the integrated absorbance values for a row of pixels that span this axis. This process was repeated for five consecutive rows and an average value calculated for each pixel position along the row to improve signal to noise. A selection of the concentration–distance profiles extracted from the imaging data are presented in Fig. 4(a)–(c) and reflect the relative concentration of PVP as a function of time.

In the absence of CO_2, the concentration–distance profiles of PVP display the characteristics of 'mutual diffusion'. Fig. 4(a) represents a situation whereby the PVP and PEG are diffusing within each other at an approximately equal rate and mutual diffusion acts to remove the inhomogeneity in the polymer system. The diffusion of glassy PVP into the liquid PEG is presumably facilitated by the act of PEG plasticising the PVP at the interfacial area, which increases the mobility of the PVP macromolecules, thus enabling the diffusion (dissolution) of PVP. The relatively low molecular weight of PEG leads to the idea of PEG diffusing through the bulk PVP on the basis of steric arguments. The sorption of CO_2 into the polymer matrix and the associated swelling is pronounced in the value of absorbance of the bulk PVP (4b–c). The principles of quantitative determination of polymer swelling from in situ ATR measurements were described for the case of conventional FTIR spectroscopy and they remain the same in the case of ATR-FTIR imaging [22]. The reduction in absorbance in the bulk PVP between the initial and subsequent profiles reflects the swelling of the matrix, which exhibits time dependence. As the polymer matrix sorbs the equilibrium fraction of CO_2, the absorbance of a polymer spectral band is reduced. This is in contrast to the system in the absence of CO_2, which, in the bulk PVP, absorbance remains unchanged. This time dependent free-volume adjustment reflects a transitional period in the chemical and physical properties of the matrix and hence a likely change in the diffusion characteristics during this time. Nevertheless, the PVP front continues to advance toward the bulk PEG after the system became equilibrated with CO_2, demonstrating that the diffusion front advancement is not due to swelling.

The reduction of non-specific chain–chain interactions by the presence of CO_2 when sorbed into a single polymer is the basis of the plasticizing ability of CO_2. In the case of interdiffusion occurring in this miscible polymer system, the role of CO_2 is more complex and time dependent with respect to each of the polymer phases. The relative affinity and solubility of CO_2 in each of the respective polymers at a specific temperature and pressure condition will dictate the rate at which the maximum weight fraction of dissolved CO_2 is approached. This translates into a difference in degree of swelling and extent of viscosity reduction between the polymer entities, which is also dependent on the molecular weight of the polymers. The diffusion behaviour displayed in a specific ternary system is complex. Prior to the acquisition of the first image in an interdiffusion experimental series, the polymer phases are contacted in the absence of CO_2, followed by a pressurisation stage. The initial contact time of the polymer phases represents the initiation of the diffusion process between the polymer phases. The extent of which diffusion occurs across the interface is determined by the molecular state of the polymer (i.e. amorphous or crystalline), molecular weight, degree of interaction, concentration of available polymer to maintain the concentration gradient, and other factors such as temperature. During the initial stages of diffusion the cell is pressurised to the required pressure. CO_2 molecules diffuse into both of the polymer phases and into the miscible region of diffused polymer (depending on the speed of the diffusion process in the absence of CO_2). As the concentration of dissolved CO_2 molecules increases to the

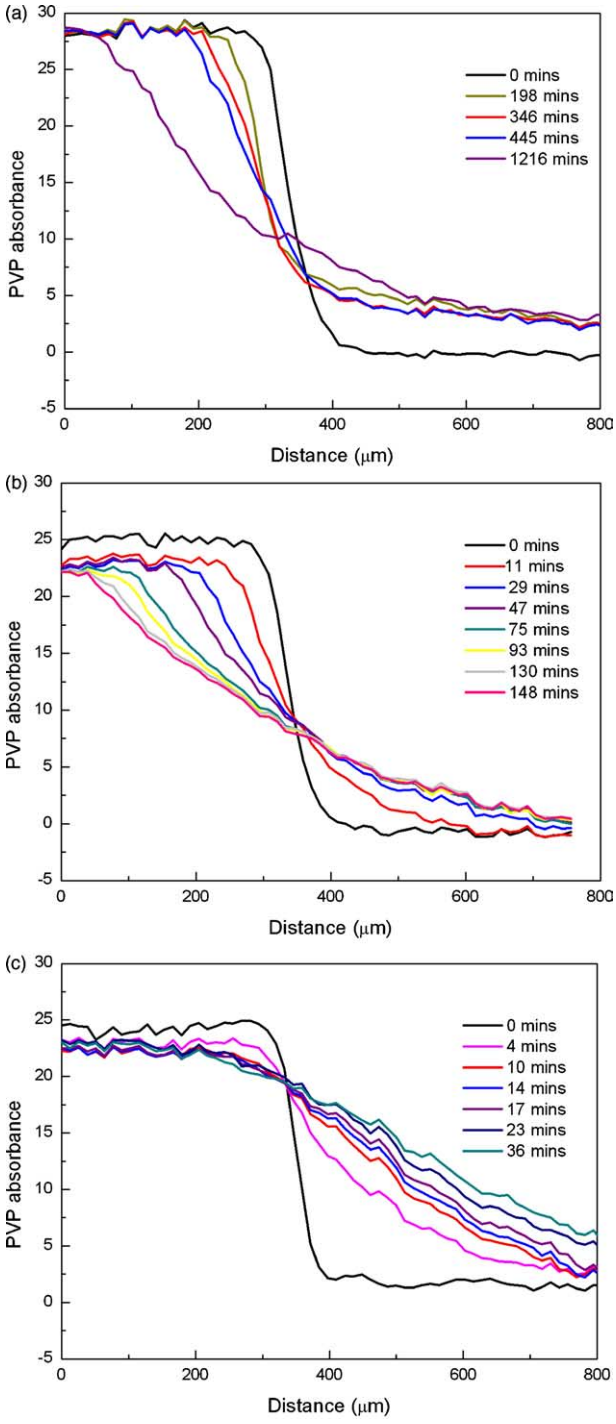

Fig. 4. (a)–(c) Extracted PVP concentration–distance profiles in contact with PEG 600 in the absence of CO_2 (a), 40 bar (b) and 80 bar (c). Each profile represents an average signal from five consecutive lines that intersect the interface perpendicularly. (For interpretation of the references in colour in this figure caption, the reader is referred to the web version of this article).

pressure specific equilibrium value, the swelling of the matrices will increase to a maximum value. It should be noted that the relative affinity of CO_2 for each of the polymers will result in favourable sorption into a specific matrix and consequently the free-volume of a specific polymer will reach its maximum value at a greater rate, as shown in Fig. 5.

The distribution of all three components measured for PEG 600 in contact with PVP at 40 bar can be visualised in the series of images presented. Inspection of Fig. 5 reveals that each of the polymer phases is seen to diffuse into the bulk of the other phase, thus confirming the phenomena of interdiffusion. The concentration of CO_2 in PEG is shown to have reached its maximum value in the first image. However, the CO_2 concentration in the PVP phase does not reach the equilibrium fraction until some time after the absorbance of CO_2 in PEG reached its maximum value, which is associated with slower diffusion of CO_2 through the PVP matrix. In addition to the difference in rate of CO_2 sorption, the equilibrium concentration of dissolved CO_2 differs between the polymers.

A qualitative comparison of the extent of swelling induced by the presence of dissolved CO_2 molecules as a function of pressure is possible with in situ ATR spectroscopy [22]. The known depth of penetration (thus the effective pathlength) of the evanescent field provides a means to measure the component concentration. The increase in free volume associated with the plasticization of the matrix decreases the concentration of polymer probed, which is reflected in the absolute absorbance in the polymer spectrum. Inspection of the images measured in the presence of CO_2 in Fig. 3 and the maximum absorbance values in the concentration plots in Fig. 4(a)–(c) reveal a decreased absorbance of PVP at 40 and 80 bar relative to atmospheric pressure (no CO_2).

3.3. Diffusion mechanism

One may assess the role of CO_2 on the interdiffusion profiles by examining the diffusion mechanism of the system. Determining the diffusion mechanism is commonly achieved using the power law shown in Eq. (1) where d is the position of the front (for 1D diffusion) after a given time t and A is a proportionality factor. Elucidation of the diffusion mechanism is possible through evaluation of the gradient of a plot of log distance vs. log time. The distance refers to the diffusing front of the polymer, which we have defined as the position where the concentration of PVP falls to ca. 75% of the maximum value. A gradient of 0.5 describes Fickian/case I diffusion in contrast to a value of 1, which corresponds to case II diffusion. Anomalous diffusion occurs when the gradient of the regression line of the measured points has an alternative value. A value greater than 1 describes a situation where the diffusion process is accelerating with time, which is normally not expected.

$$d = At^{\alpha} \tag{1}$$

The log distance vs. log time plots for PVP in contact with PEG in the absence of CO_2, at 40 and 80 bar are presented in Fig. 6. Equations for corresponding to the specific linear fits of the data points are included in the Fig. 6 of which the gradients describe the diffusion mechanism. In the absence of CO_2, the diffusion mechanism is described by the case II mechanism and becomes more Fickian (case I) with increasing pressure. The fact that the diffusion behaviour becomes more Fickian in

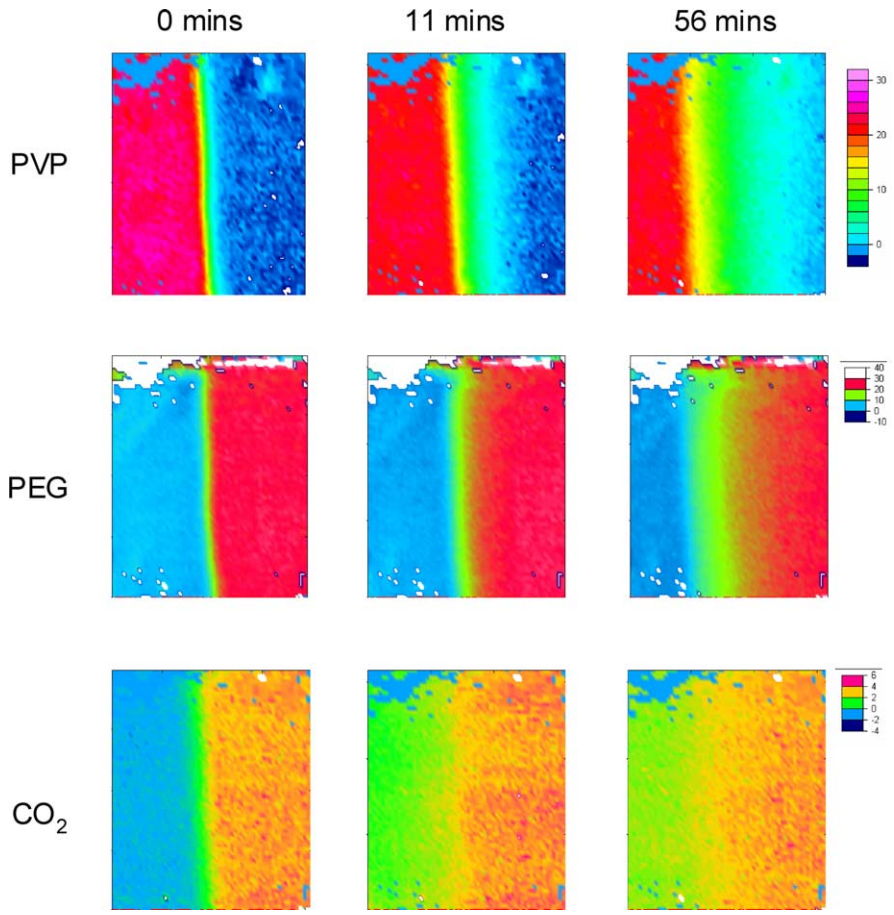

Fig. 5. ATR-FTIR images corresponding to PVP in contact with PEG 600 at 40 bar corresponding to PVP (top), PEG (middle) and dissolved CO_2 (bottom). For a specific time all of the images were generated from the same measurement using the distribution of the characteristic spectral feature associated with each component.

character with increasing pressure is consistent with the expected increase in plasticization offered by CO_2 dissolved in polymer at greater weight fractions. The increase in polymer free-volume increases the distance between neighbouring chains in addition to the proximity that segments of the same macromolecule may occupy, which contribute to enhanced conformational mobility/relaxation. Under such conditions the time scale for conformational adjustment is small in comparison with the characteristic timescale for diffusion, which results in a Deborah number significantly lower than 1 and hence Fickian diffusion. The transition from a case II to case I mechanism is a consequence of free-volume/chain mobility alterations.

The same analysis procedure was performed on imaging data sets for PVP in contact with PEG 1500. PEG 1500 has a semi-crystalline morphology and when in contact with PVP at 35 °C, no interdiffusion was observed in 100 h. However, exposure to the same system in the presence of CO_2 results in significant interdiffusion, and thus CO_2 not only accelerates the process, but actually facilitates its occurrence. CO_2 is able to initiate interdiffusion by lowering the melting temperature of the PEG crystallites [30,31] and thus mimicking the effect of heat. The nature of CO_2 sorption into the PEG matrix is depicted in Fig. 7 where PEG 1500 in contact with PVP at 40 bar measured directly after the pressurisation procedure was complete. All three images were generated from the same measurement but different characteristic absorption bands were used to represent the distribution of

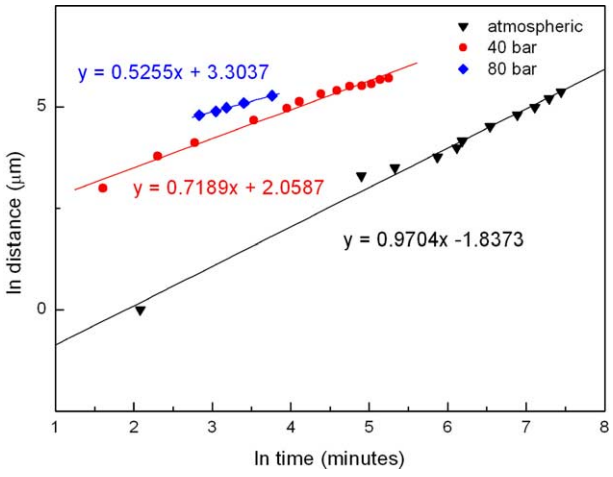

Fig. 6. Plot of logarithm distance vs. logarithm time for PVP in contact with PEG 600 in the absence of CO_2, at 40 and 80 bar. The distance of the PVP corresponds to the position on the concentration profile where the absorbance falls to ca. 75% of its maximum value. The gradient of the linear regression is indicative of the diffusion mechanism.

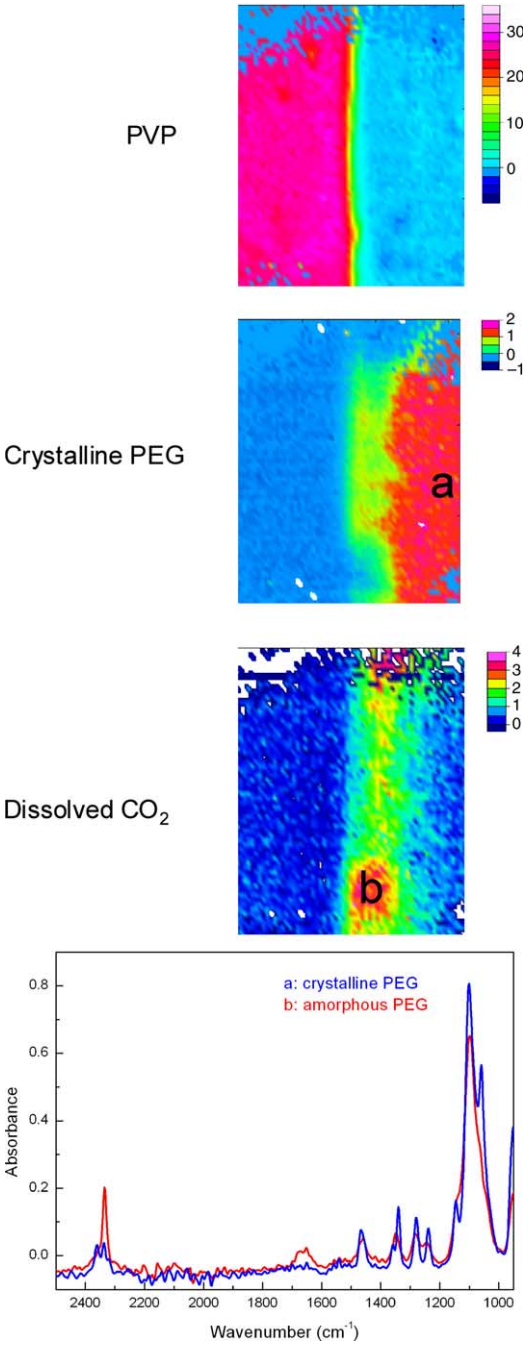

Fig. 7. ATR-FTIR images corresponding to PVP in contact with PEG 1500 at 40 bar of CO_2 shortly after pressurisation. All of the images were generated from the same measurement and integrated for each of the three components. The spectra shown were extracted from the two positions labelled (a and b).

PVP, crystalline PEG and dissolved CO_2. CO_2 is found to reside mostly within the PEG domain close to the polymer interfacial region. The initial absence of CO_2 in the bulk PVP is related to the relative affinity of CO_2 to the polymer entities and the time required to reach the area of polymer adjacent to the diamond. The CO_2 distribution coincides with the distribution of largely amorphous PEG, which is evidenced in the spectrum extracted from the interfacial region (labelled b on image). The PEG in that region displays spectral features characteristic of amorphous PEG in addition to the presence of dissolved CO_2 molecules. This provides evidence that the relatively high CO_2 concentration in this region is not attributed to a void in the polymer system that is simply filled with the surrounding CO_2 but reflects CO_2 molecules that are dissolved within the largely amorphous polymer matrix. The spectrum extracted from the bulk PEG region is characteristic of largely crystalline PEG 1500 and is devoid of from the spectral features of dissolved CO_2. Inspection of the spectrum merely reveals the presence of gaseous CO_2, which is attributed to gaseous CO_2 in the measurement path that was not completely compensated by the background measurement. The presence of CO_2 at the interfacial region of the polymer system may be rationalised by the relatively low level of structural integrity of the PEG crystallites at the interface with PVP compared to the bulk PEG crystallites. On this basis, the access of CO_2 into the PEG phase is possible, which enables the melting of the crystallites and promotes interdiffusion, which is not observable under atmospheric conditions. Concentration–distance profiles were extracted from the imaging datasets in an identical manner to the PEG 600 data and are presented in Fig. 8(a) and (b).

Fig. 9 shows that the plot of the logarithm of diffusion front distance vs. logarithm of time (Log distance − Log time) at 40 bar has a gradient of greater than 1, which implies the

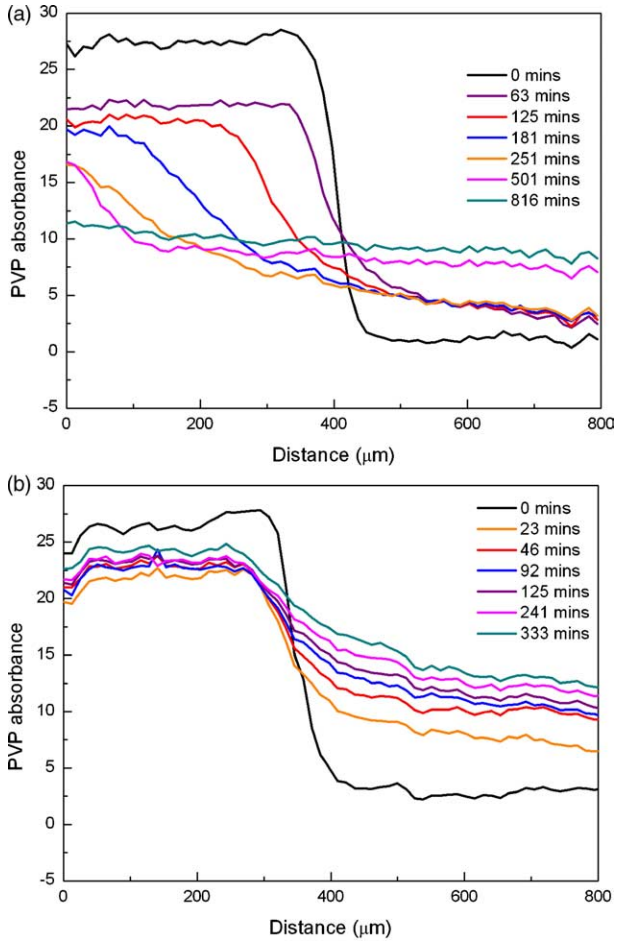

Fig. 8. (a) and (b). Extracted PVP concentration–distance profiles in contact with PEG 1500 at 40 bar (a) and 80 bar (c). Each profile represents an average signal from five consecutive lines that intersect the interface perpendicularly.

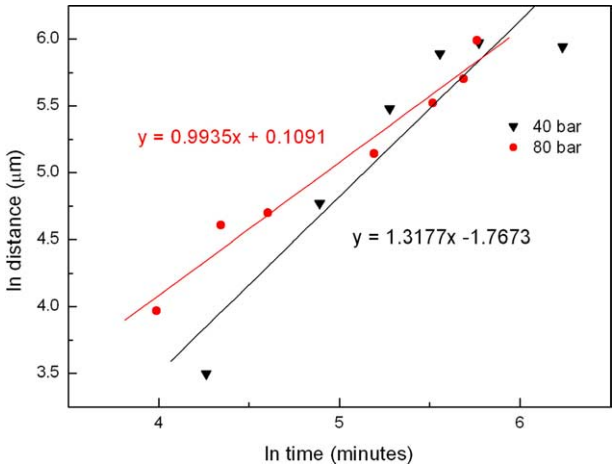

Fig. 9. Plot of logarithm distance vs. logarithm time for PVP in contact with PEG 1500 subjected to 40 and 80 bar of CO_2. The distance of the PVP corresponds to the position on the concentration profile where the absorbance falls to ca. 75% of its maximum value. The gradient of the linear regression is indicative of the diffusion mechanism.

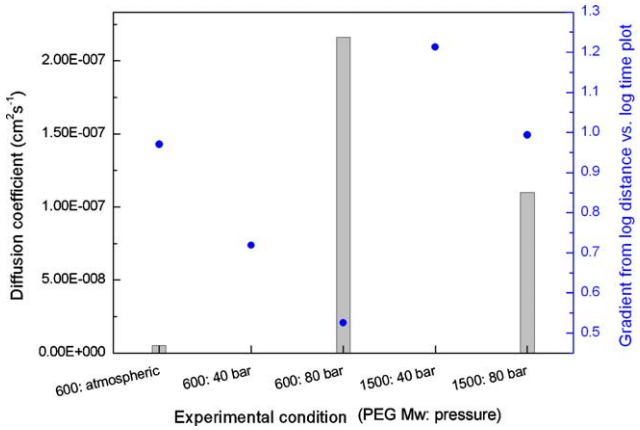

Fig. 10. Summary of diffusion coefficient and exponent of log-distance vs. log-time plot. (characteristic of diffusion mechanism) for each experimental condition. Grey bars represent the diffusion coefficient while dots represent the gradient from the log distance vs. log time plots (For interpretation of the references in colour in this figure caption, the reader is referred to the web version of this article).

diffusion increases in speed as a function time. A possible explanation for this behaviour is due to the dramatic changes in the free-volume of the PEG during the transition in morphology from crystalline to amorphous. The density of the PEG crystallites are relatively high [32] which corresponds to a low degree of free-volume. As the crystallites melt due to the sorption of CO_2, the free-volume increases in a time dependent manner due to the kinetics of the morphological transition, which accompanies crystallite melting combined with the diffusion of CO_2 through the polymer. This is a plausible explanation for the diffusion mechanism. At 80 bar the diffusion mechanism does not show an increase in speed presumably due to the rapid melting of the crystallites at higher pressure. The fact that case II behaviour is observed may be explained by the molecular weight of PEG. The amount of chain entanglement in the bulk PEG 1500 will be considerably greater than in the lower molecular weight PEG even in the presence of CO_2. The advance of PVP into the bulk PEG requires the coordinated movement of PEG macromolecules to accommodate the passage of PVP, which is likely to be more hampered at higher molecular weights and thus the time scale for conformational change is likely to be greater.

3.4. Diffusion coefficient estimation

For one-dimensional diffusion, a plot of the square root of time vs. distance moved by the PVP front provides the required information to calculate the diffusion coefficient from the experimental data. The calculated diffusion mechanism (1 = case II and 0.5 = case I) are summarised in Fig. 10. The diffusion coefficient for those systems which undergo case I and case II diffusion mechanisms have been calculated and presented in Fig. 10. In all cases the presence of CO_2 accelerates the interdiffusion relative to the reference data of PEG 600 under atmospheric conditions. Increasing the CO_2 pressure is seen to accelerate the interdiffusion demonstrating the opportunity to 'tune' the interdiffusion process. The validity of our approach may be assessed through a comparison of the calculated diffusion coefficient in the absence of CO_2 with a literature value. Bairamov et al. [24] studied the interdiffusion of PVP (K17-molecular weight is 9000) in contact with PEG 400 at 25 °C and reported a diffusion coefficient of 6.6×10^{-10} cm^2 s^{-1}. The value calculated in this work for PVP (K15) in contact with PEG 600 at 35 °C of 5.2×10^{-9} cm^2 s^{-1} gives us confidence in our experimental approach as the diffusion coefficient is expected to increase on the basis of temperature, PVP molecular weight and the reduced 'molecular friction' (relating to formation of hydrogen bonding between a solute and polymer matrix) associated with increasing PEG molecular weight. The reduction of 'molecular friction' present may enable the progression of PEG 1500 in a less hindered manner than 600, which interacts with PVP more strongly. This highlights the importance of considering both the molecular dimensions of the components of the system and the strength of the interaction.

3.5. Specific intermolecular interactions

The advantage of FTIR spectroscopy is the ability to examine the system at the molecular level and hence evaluate intermolecular interactions. Such an analysis allows one to relate the observed bulk diffusion characteristics with intermolecular interactions occurring in the ternary system. Our analysis focuses on the ν(C=O) of PVP due to the involvement of the oxygen atom of the carbonyl group of PVP in hydrogen bonding with the terminal OH groups of PEG [1]. The presence of the hydrogen bonding results in the shift of the ν(C=O) band to the lower-wavenumber region.

To assess the strength of interaction occurring between the polymers, spectra have been extracted from the interfacial

areas, which contain all three components of the system. The ν(C=O) region corresponding to spectra extracted from the interfacial regions of images that were measured after the equilibrium concentration of CO_2 had been achieved are shown in Fig. 11. The observed changes in the spectral features of the ν(C=O) band are due to a contribution from hydrogen bonding and the weak Lewis acid–base interactions with the CO_2 as was demonstrated in a similar system previously [1]. In this respect, the carbonyl oxygen of PVP can be considered as a competitive interaction site at which a stoichiometric ratio of PEG and CO_2 interactions should be dependent on both CO_2 pressure and molecular weight of PEG due to the number of terminal hydroxyl groups. Inspection of the spectra shown in Fig. 11 reveals that the ν(C=O) indeed is sensitive to these variables as seen by the unique band shape under different conditions. Each of the bands is a manifestation of carbonyl groups that are: not involved in bonding (free carbonyls), a proportion that are participating in hydrogen bonding with PEG, and those that are interacting with CO_2. In the absence of high-pressure CO_2 (PVP with PEG 600) the ν(C=O) band appears to be formed of two features, presumably the 'free' or weakly interacting carbonyl group (1671 cm^{-1}) and the hydrogen-bonded component (1656 cm^{-1}). The position of these bands are consistent with those reported for the complex formation between PVP and PEG 400 in the absence of carbon dioxide [25,26]. At this condition the spectrum shows the largest contribution from the hydrogen-bonded carbonyls. This confirms that the amount of hydrogen-bonding is greater with PEG 600 compared to 1500 as a result of the number of the terminal hydroxyl functionalities available. In the presence of CO_2 the relative ratio of the two components changes, which may be attributed to the competition of CO_2 interacting with the carbonyl group of the PVP molecules. The number of hydrogen-bonded carbonyl groups is reduced at greater pressure, indicated by the reduction in the absorption band (1656 cm^{-1}) as a function of increasing pressure (80 bar shows the lowest degree of hydrogen bonding). This is molecular level evidence for the origin of the observed increase in diffusion coefficient of PEG 600 with increasing CO_2 pressure as not only does the increase in free-volume act to accelerate the transport by 'molecular lubrication' but additionally the degree of 'molecular friction' occurring between the polymeric components via H-bonding is reduced. As expected, the changes of the ν(C=O) bands shown for PEG 1500 confirm that the extent of hydrogen bonding is significantly reduced in comparison with PEG 600 (Fig. 11).

This reduction in extent of hydrogen bonding with PEG 1500 may explain the similar diffusion coefficient observed for PEG 1500 at 40 bar and PEG 600 at the same conditions. The reduction of 'molecular friction' provided may enable the progression of PEG 1500 in a less hindered manner than PEG 600, which interacts with PVP more strongly. This is not observed at 80 bar due to the carbonyl groups being sufficiently shielded by CO_2 hence PEG 600 diffuses at a significantly accelerated rate. The effect of CO_2-enhanced diffusion of PEG in PVP is similar to that observed for the enhancement of diffusion of dyes in other glassy polymers [33], however, it is the first time that this effect was related to polymer interdiffusion, which was visualised with spectroscopic imaging.

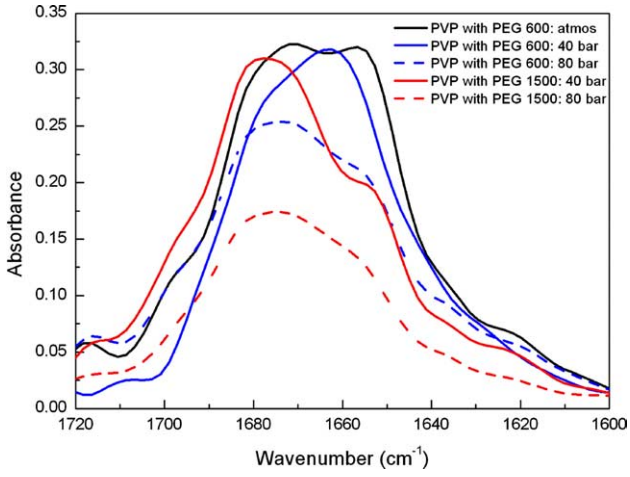

Fig. 11. ATR-FTIR spectra of PVP in the ν(C=O) region extracted from the interfacial region with PEG for the experimental conditions indicated.

4. Discussion and conclusions

The application of in situ ATR-FTIR spectroscopic imaging has been realised to investigate the interdiffusion process in a miscible polymer system (PVP/PEG) in the presence of high-pressure and supercritical CO_2. This chemical imaging approach allowed us to study a dynamic system in situ and to simultaneously measure the spatial distribution of both polymers and CO_2 as a function of time. The presence of CO_2 molecules dissolved in the polymer system has been shown to significantly enhance the interdiffusion process under isothermal conditions, and was studied as a function of pressure and PEG molecular weight. Pressure control has been demonstrated as an effective measure to 'tune' the speed of the interdiffusion process. Control over the diffusion characteristics by pressure regulation, in combination with in situ ATR FTIR imaging, provides a powerful combination to guide to processing requirements of a specific system. The chemical specificity offered by FTIR spectroscopic imaging enables the bulk behaviour of the system to be interrelated to molecular level information, which offers an in-depth picture of the dynamic system. Further opportunities exist in applications of in situ FTIR spectroscopic imaging to high-pressure CO_2-induced phase separation, mixing, blending, diffusion, impregnation and foaming.

Acknowledgements

We thank EPSRC and European Commission (SurfaceT project NMP2-CT-2005-013524) for support.

References

[1] Kazarian SG, Martirosyan GG. Int J Pharm 2002;232(1/2):81–90.
[2] Royer JR, Gay YJ, DeSimone JM, Khan SA. J Polym Sci, Part B: Polym Phys 2000;38(23):3168–80.

[3] Garcia-Leiner M, Lesser AJ. J Appl Polym Sci 2004;93:1501–11.
[4] Martinache JD, Royer JR, Siripurapu S, Hénon FE, Genzer J, Khan SA, et al. Ind Eng Chem Res 2001;40:5570–7.
[5] Han X, Koelling KW, Tomasko DL, Lee LJ. Polym Eng Sci 2002;42(11): 2094–106.
[6] Handa P, Zhang Z. Macromolecules 2000;38(5):716–25.
[7] Krause B, Diekmann K, van der Vegt NFA, Wessling M. Macromolecules 2002;35:1738–45.
[8] Kung E, Lesser AJ, McCarthy TJ. Macromolecules 2000;33(22):8192–9.
[9] Watkins JJ, McCarthy TJ. Macromolecules 1994;27(17):4845–7.
[10] Gupta RR, Lavery KA, Francis TJ, Webster JRP, Smith GS, Russell TP, et al. Macromolecules 2003;36:346–52.
[11] Harton SE, Stevie FA, Spontak RJ, Koga T, Rafailovich MH, Sokolov JC, et al. Polymer 2005;46:10173–9.
[12] Koga T, Seo YS, Hu X, Shin K, Zhang Y, Rafailovich MH, et al. Europhys Lett 2002;60:559–65.
[13] Thompson RL, McDonald MT, Lenthall JT, Hutchings LR. Macromolecules 2005;38:4339–44.
[14] Snively CM, Koenig JL. J Polym Sci B: Polym Phys 1999;37:2261–8.
[15] Miller-Chou BA, Koenig JL. Macromolecules 2002;35:440–4.
[16] Koenig J. Adv Mater 2002;14:457–60.
[17] Bobiak Jp, Koenig JL. Appl Spectrosc 2004;58:1141–6.
[18] Kazarian SG, Chan KLA. Macromolecules 2003;36:9866–72.
[19] Kazarian SG, Kong KWT, Bajomo M, Van der Weerd J, Chan KLA. Food Bioproducts Process 2005;83(C2):127–35.
[20] Chan KLA, Kazarian SG. Appl Spectrosc 2003;57:381–9.
[21] Kazarian SG, Chan KLA. Macromolecules 2004;37:579–84.
[22] Flichy NMB, Kazarian SG, Lawrence CJ, Briscoe BJ. J Phys Chem B 2002;106:754–9.
[23] Bairamov DF, Chalykh AE, Feldstein MM, Siegel RA. Macromol Chem Phys 2002;203(18):2674–86.
[24] Bairamov DF, Chalykh AE, Feldstein MM, Siegel RA. J Appl Polym Sci 2002;85:1128–36.
[25] Feldstein MM, Lebedeva TL, Shandryuk GA, Kotomin SV, Kuptsov SA, Igonin VE, et al. Vusokomoleculyarnue Soed. Ser. A. 1999;41:1316–30.
[26] Feldstein MM, Lebedeva TL, Shandryuk GA, Igonin VE, Avdeev NN, Kulichikhin VG. Vusokomoleculyarnue Soed Ser A 1999;41:1331–40.
[27] Burka EM, Curbelo R, US Patent 6, 141, 100;2000.
[28] Matsuura H, Miyazawa T. J Polym Sci, Part A-2: Polym Phys 1969;7(10): 1735–44.
[29] Kazarian SG, Vincent MF, Bright FV, Liotta CL, Eckert CA. J Am Chem Soc 1996;118:1729–36.
[30] Kazarian SG. Macromol Symp 2002;184:215–28.
[31] Wiesmet V, Weidner E, Behme S, Sadowski G, Artl W. J Supercrit Fluids 2000;17:1.
[32] Bandrup J, Immergut EH, Grulke EA. Polymer Handbook. Nomenclature. New York: Wiley; 1999.
[33] West BL, Kazarian SG, Vincent MF, Brantley NH, Eckert CA. J Appl Polym Sci 1998;69:911–9.